Applied Thermal Engineering 127 (2017) 559–565

Contents lists available at ScienceDirect

Applied Thermal Engineering

journal homepage: www.elsevier.com/locate/apthermeng

Research Paper

Performance analysis of perovskite and dye-sensitized solar cells under varying operating conditions and comparison with monocrystalline silicon cell

Sourav Khanna [a,*], Senthilarasu Sundaram [a], K.S. Reddy [b], Tapas K. Mallick [a,*]

[a] Environment and Sustainability Institute, Penryn Campus, University of Exeter, Cornwall TR10 9FE, United Kingdom
[b] Heat Transfer and Thermal Power Laboratory, Department of Mechanical Engineering, Indian Institute of Technology Madras, Chennai 600 036, India

HIGHLIGHTS

- When perovskite reaches 53 °C, dye-sensitized reaches 57 °C and mono-Si reaches 61 °C.
- Decrease in wind azimuth increases perovskite cell's efficiency from 19.5% to 20.1%.
- Increase in wind velocity decreases perovskite cell's temperature from 53 °C to 44 °C.

ARTICLE INFO

Article history:
Received 23 January 2017
Revised 11 June 2017
Accepted 5 August 2017
Available online 12 August 2017

Keywords:
Perovskite
Dye sensitized
Temperature
Thermal analysis

ABSTRACT

The efficiency of solar cell is generally defined at standard test conditions. However, wind direction, wind velocity, tilt angle of panel and solar radiation during operation differ from those at standard test conditions. The effects of operating conditions on the temperature and efficiency of silicon solar cells are widely analysed in literature. In the current work, the thermal performance of perovskite and dye-sensitized solar cells in operating conditions has been analysed and compared with monocrystalline silicon solar cell. The effects of wind direction (wind azimuth angle), wind velocity, tilt angle of panel and solar radiation on the temperature and efficiency of the cells have been analysed. The results show that as wind azimuth angle increases from 0° to 90°, the temperature of the cell increases from 51.8 °C to 58.2 °C for monocrystalline silicon, from 45.5 °C to 50.7 °C for perovskite and from 48.4 °C to 53.9 °C for dye-sensitized solar cell and the corresponding efficiency of the cell decreases from 22.3% to 21.5% for monocrystalline silicon, from 20.1% to 19.5% for perovskite and from 11.8% to 11.7% for dye-sensitized solar cell.

1. Introduction

Solar photovoltaic is one of the fastest growing renewable technologies. However, in solar cells, only a fraction of the incident solar radiation gets converted into electricity. Rest of the solar radiation gets converted into heat and raises the temperature of the cell. The temperature rise affects the efficiency (solar radiation to electricity conversion) of the cell. The efficiency of solar cells is generally defined at standard test conditions. However, ambient and operating conditions differ from those of standard test conditions.

For silicon solar cells, many studies are available in literature for finding the temperature of the cell in operating conditions and its effect on the efficiency of the cell which are as follows: Skoplaki and Palyvos [1] presented the available correlations for finding the temperature of the cell as function of solar radiation, ambient temperature and wind velocity. Kaplani and Kaplanis [2] incorporated the effect of wind direction and module tilt on the temperature of the cell. Skoplaki et al. [3] provided the correlations for cell temperature for various mounting conditions of the module, viz. free standing, flat roof, sloped roof and façade integrated. Skoplaki and Palyvos [4] presented the available correlations for finding the efficiency as function of temperature of the cell. Lu and Yao [5] presented the thermal analysis of the cell considering arbitrary number of glass layers. All the above studies consider steady state analysis whereas Jones and Underwood [6] and Armstrong and Hurley [7] carried out transient analysis in which the former

* Corresponding authors.
E-mail addresses: s.khanna@exeter.ac.uk (S. Khanna), t.k.mallick@exeter.ac.uk (T.K. Mallick).

http://dx.doi.org/10.1016/j.applthermaleng.2017.08.030
1359-4311/

Nomenclature

A_i	parameter appeared in Eq. (16) (K/m)
B_i	parameter appeared in Eq. (16) (K)
F	view factor between surfaces
Gr	Grashof number
h	convective heat transfer coefficient (W/m^2 K)
I_T	solar radiation on tilted surface (W/m^2)
k	thermal conductivity (W/m K)
L	length (m)
L_{ch}	characteristic length (m)
Pr	Prandtl number of air
Ra	Rayleigh number
Re	Reynolds number
S_h	solar radiation converted into heat (W/m^2)
t	thickness of the cell (m)
T	temperature (K)
U	overall heat transfer coefficient (W/m^2 K)
v_w	wind velocity (m/s)
w	width (m)

Greek symbols

β	tilt angle of the panel (rad)
γ_w	wind azimuth angle i.e. the angle made by wind stream with the projection of surface normal on horizontal plane (rad)
ε	emissivity for long wavelength radiation
η_{cell}	solar radiation to electricity conversion efficiency of the cell
σ	Stefan–Boltzmann constant (W/m^2 K^4)
$(\tau\alpha)_{eff}$	effective product of transmissivity of glass cover and absorptivity of solar cell
υ	kinematic viscosity of air (m^2/s)

Abbreviation

DSSC	dye-sensitized solar cell
EVA	ethylene vinyl acetate

Subscripts

a	ambient
b	bottom surface of the cell
c	critical
for	forced convection
g	ground
i	ith layer of the cell
nat	natural convection
s	sky
t	top surface of the cell

considered lumped model for cell materials and the latter considered each layer of the cell separately.

For dye-sensitized solar cells (DSSC), Grätzel [8] reported that the temperature of the cell does not affect the solar to electricity conversion efficiency. Raga and Santiago [9] reported that the DSSC efficiency remains almost constant with maximum around 30–40 °C. However, Sebastian et al. [10] reported that, above room temperature, DSSC efficiency decreases with increase in cell temperature and for very low temperatures (<0 °C), efficiency increases with temperature. Pettersson et al. [11] presented the performance of low powered DSSC module and found that, below room temperature, efficiency increases with temperature and, above room temperature, it decreases with temperature. Chen et al. [12] presented the thermal analysis of the DSSC module. Pan et al. [13] analysed the performance of DSSC module integrated with cooling system for thermal management of the cells. Berginc et al. [14,15] studied the effects of temperature and iodine concentration on the performance of DSSC and reported the experimental measurements. Tripathi et al. [16] modelled the DSSC system and predicted the performance of DSSC under various levels of illumination and cell temperature. Zhang et al. [17] analysed the effect of temperature on the efficiency of perovskite solar cells. Cojocaru et al. [18] presented the effect of temperature on the crystal structure and the performance of perovskite cells.

Thus, it can be concluded that the performance of silicon solar cells in operating conditions is widely analysed. However, the study related to the effect of operating conditions on the temperature and efficiency of perovskite and dye-sensitized solar cells is not available in literature and, thus, it has been carried out in the current work.

2. Methodology

Solar cell having length L, width w and thickness t is considered in this work. The geometry of the cell is defined by cartesian coordinates (x, y, z) with centre at O (0, 0, 0) as shown in Fig. 1. Three types of solar cells: perovskite, dye-sensitized and monocrystalline silicon cells are considered. The perovskite cell is considered to be made up of five layers. 1st layer ($0 \le z \le t_1$) is glass, 2nd layer ($t_1 \le z \le t_2$) is TiO_2, 3rd layer ($t_2 \le z \le t_3$) is perovskite, 4th layer ($t_3 \le z \le t_4$) is Spiro-OMeTAD and 5th layer ($t_4 \le z \le t_5$) is silver. The layers of dye-sensitized solar cell are glass, dye sensitized TiO_2, electrolyte, platinum and glass. The layers of monocrystalline silicon solar cell are glass, ethylene vinyl acetate (EVA), silicon, EVA and tedlar.

The following assumptions have been made in this work

(i) The heat losses from the top and bottom surfaces are only considered and from the sides are neglected as the thickness of the cell is negligible compared to its length and width.
(ii) Due to very small thickness of cell's layers (nm-μm), the contact resistances hardly affect the average temperature of the cell. Thus, they are not considered in the thermal analysis which helps in keeping the model simple.
(iii) Since the thickness of the cell is very less, thermal capacity of the cell is neglected.

The fraction of the incident solar radiation (I_T) that gets transmitted through the glass cover and absorbed by the solar cell can be written as $(\tau\alpha)_{eff}$ x I_T where $(\tau\alpha)_{eff}$ is the effective product of transmissivity of glass cover and absorptivity of solar cell. Out of the absorbed one, only a small portion gets converted into electricity and the rest of the solar radiation gets converted into heat (S_h) which can be written as

$$S_h = (\tau\alpha)_{eff} I_T - \eta_{cell} I_T \tag{1}$$

where η_{cell} is the solar radiation to electricity conversion efficiency of the cell. At the interface of the 2nd and 3rd layers (i.e. at $z = t_2$), the heat (S_h) flows towards the top and bottom of the cell. Thus, at $z = t_2$, the sum of flow rates of heat entering the 2nd and 3rd layers can be written as follows

$$\left[k_2 \frac{\partial T_2}{\partial z}_{at\ z=t_2}\right] + \left[-k_3 \frac{\partial T_3}{\partial z}_{at\ z=t_2}\right] = S_h \tag{2}$$

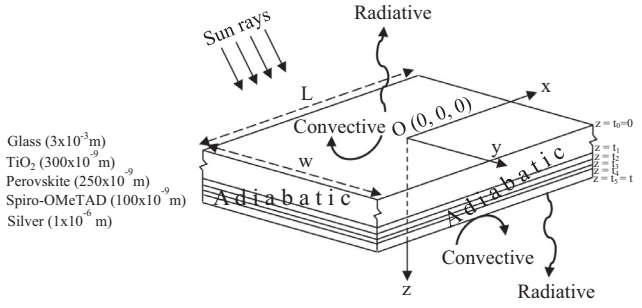

(a) Perovskite solar cell

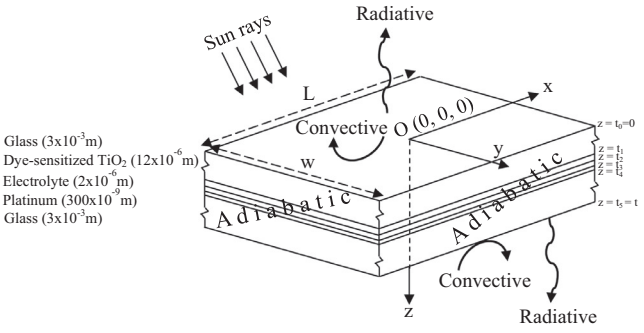

(b) Dye-sensitized solar cell

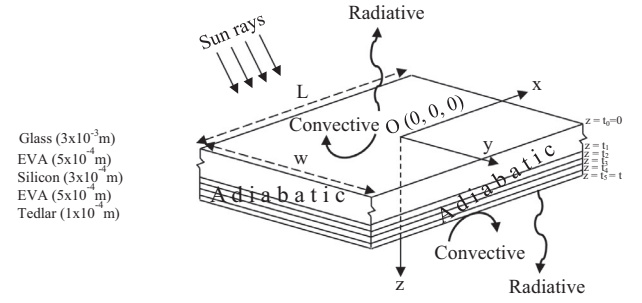

(c) Monocrystalline silicon solar cell

Fig. 1. View of the coordinate system defining the geometry of the cells.

where k_2 and k_3 are the thermal conductivities of the 2nd and 3rd layers respectively. During steady state, the heat conducts through each ith layer (i = 1 to 5) following the below equation

$$\frac{\partial^2 T_i}{\partial z^2} = 0;\ for\ i = 1\ to\ 5 \tag{3}$$

At the interface of the i^{th} and $(i+1)^{th}$ layers (i.e. at $z = t_i$), the flow rate of heat leaving the i^{th} layer is same as the flow rate entering the successive layer. Thus, the following energy balance can be written

$$k_i \frac{\partial T_i}{\partial z}_{at\ z=t_i} = k_{i+1} \frac{\partial T_{i+1}}{\partial z}_{at\ z=t_i};\quad for\ i = 1, 3\ and\ 4 \tag{4}$$

where k_i is the thermal conductivity of the i^{th} layer. Temperature of the i^{th} and $(i+1)^{th}$ layers at their interface (i.e. at $z = t_i$) is same. Thus,

$$T_{i_{at\ z=t_i}} = T_{i+1_{at\ z=t_i}};\quad for\ i = 1\ to\ 4 \tag{5}$$

From the top and bottom surfaces, heat is lost to surroundings due to convective and radiative losses. Thus, at $z = 0$ and $z = t_5$, the following energy balances can be written

$$k_1 \frac{\partial T_1}{\partial z}_{at\ z=0} = h_t[T_{at\ z=0} - T_a] + \sigma \varepsilon_t F_{t\_s}\left[T^4_{at\ z=0} - T^4_s\right] + \sigma \varepsilon_t F_{t\_g}\left[T^4_{at\ z=0} - T^4_g\right] \tag{6}$$

$$-k_5 \frac{\partial T_5}{\partial z}_{at\ z=t_5} = h_b[T_{at\ z=t_5} - T_a] + \sigma \varepsilon_b F_{b\_s}\left[T^4_{at\ z=t_5} - T^4_s\right] + \sigma \varepsilon_b F_{b\_g}\left[T^4_{at\ z=t_5} - T^4_g\right] \tag{7}$$

where k_1 and k_5 are the thermal conductivities of the 1st and 5th layers respectively. h_t and h_b are the convective heat transfer coefficients of the top and bottom surfaces respectively. T_a is ambient temperature. σ is Stefan–Boltzmann constant. ε_t and ε_b are the emissivities for long wavelength radiation of the top and bottom surfaces respectively. F_{t_s}, F_{t_g}, F_{b_s} and F_{b_g}, are the view factors between top surface and sky, top surface and ground, bottom surface and sky, and bottom surface and ground respectively. T_s and T_g are the sky and ground temperature respectively. Following Kaplani and Kaplanis [2], h_t can be written as combination of natural and forced convection as follows

$$h_t = \begin{cases} h_{t\_for}; & if\ Gr/Re^2 \leqslant 0.01 \\ \left|h^{7/2}_{t\_nat} + h^{7/2}_{t\_for}\right|^{2/7}; & if\ 0.01 < Gr/Re^2 < 100, \beta = 0^\circ \\ \left|h^{3}_{t\_nat} + h^{3}_{t\_for}\right|^{1/3}; & if\ 0.01 < Gr/Re^2 < 100, \beta > 0^\circ \\ h_{t\_nat}; & if\ Gr/Re^2 \geqslant 100 \end{cases} \tag{8}$$

where Gr is Grashof number, Re is Reynolds number and β is the tilt angle of the panel. h_{t_nat} and h_{t_for} are the heat transfer coefficients of the top surface due to natural and forced convection respectively and can be written as follows

$$h_{t\_nat} = \begin{cases} \left[0.13\left\{(GrPr)^{1/3} - (Gr_cPr)^{1/3}\right\} + 0.56(Gr_cPr\sin\beta)^{1/4}\right]k_a/L_{ch}; & if\ \beta > 30^\circ \\ \left[0.13(GrPr)^{1/3}\right]k_a/L_{ch}; & if\ \beta \leqslant 30^\circ \end{cases} \tag{9}$$

$$h_{t\_for} = 0.848 k_a[\sin\beta \cos\gamma_w v_w Pr/\upsilon]^{0.5}(L_{ch}/2)^{-0.5} \tag{10}$$

where Pr is Prandtl number of air, Gr_c is the critical Grashof number = $1.327 \times 10^{10}\ \exp\{-3.708(\pi/2\text{-}\beta)\}$, L_{ch} is the characteristic length i.e. the length of surface along the direction of air flow, k_a is the thermal conductivity of air, γ_w is the wind azimuth angle (the angle made by wind stream with the projection of surface normal on horizontal plane), v_w is the wind velocity, υ is kinematic viscosity of air. Following Kaplani and Kaplanis [2], h_b can be written as combination of natural and forced convection as follows

$$h_b = \begin{cases} h_{b\_for}; & if\ Gr/Re^2 \leqslant 0.01 \\ \left|h^{7/2}_{b\_nat} \pm h^{7/2}_{b\_for}\right|^{2/7}; & if\ 0.01 < Gr/Re^2 < 100, \beta = 0^\circ \\ \left|h^{3}_{b\_nat} \pm h^{3}_{b\_for}\right|^{1/3}; & if\ 0.01 < Gr/Re^2 < 100, \beta > 0^\circ \\ h_{b\_nat}; & if\ Gr/Re^2 \geqslant 100 \end{cases} \tag{11}$$

In the above equation, '+' is used when natural and forced flow are assisting each other and '−' is used when they are opposing. Thus, if back side of the panel is leeward, '+' is used and if it is wind ward, '−' is used. h_{b_nat} and h_{b_for} are the heat transfer coefficients of the bottom surface due to natural and forced convection respectively and can be written as follows

$$h_{b\_nat}\begin{cases} 0.58(Ra)^{1/5}k_a/L_{ch}; & \text{if } \beta \leqslant 2^\circ \\ 0.56(Ra\sin\beta)^{1/5}k_a/L_{ch}; & \text{if } 2^\circ < \beta < 30^\circ \\ \left[0.825+\frac{0.387(Ra\sin\beta)^{1/6}}{\left\{1+(0.492/Pr)^{9/16}\right\}^{8/27}}\right]^2 k_a/L_{ch}; & \text{if } \beta \geqslant 30^\circ \end{cases} \quad (12)$$

$$h_{b\_for}=\begin{cases} 5.74v_w^{0.8}L_{ch}^{-0.2}; & \text{if } Re_c\upsilon/v_wL_{ch} \leqslant 0.05 \\ 5.74v_w^{0.8}L_{ch}^{-0.2}-16.46L_{ch}^{-1}; & \text{if } 0.05 < Re_c\upsilon/v_wL_{ch} < 0.95 \\ 3.83v_w^{0.5}L_{ch}^{-0.5}; & \text{if } Re_c\upsilon/v_wL_{ch} \geqslant 0.95 \end{cases} \quad (13)$$

where Ra is Rayleigh number, L_{ch} is the characteristic length i.e. the length of surface along the direction of air flow and Re_c is the critical Reynolds number (= 4×10^5).

By combining the convective and radiative heat transfer, overall heat transfer coefficients of the top and bottom surfaces (U_t and U_b) are defined as follows

$$U_t[T_{at\ z=0}-T_a]=h_t[T_{at\ z=0}-T_a]+\sigma\varepsilon_tF_{t\_s}\left[T_{at\ z=0}^4-T_s^4\right]+\sigma\varepsilon_tF_{t\_g}\left[T_{at\ z=0}^4-T_g^4\right] \quad (14)$$

$$U_b[T_{at\ z=t_5}-T_a]=h_b[T_{at\ z=t_5}-T_a]+\sigma\varepsilon_bF_{b\_s}\left[T_{at\ z=t_5}^4-T_s^4\right]+\sigma\varepsilon_bF_{b\_g}\left[T_{at\ z=t_5}^4-T_g^4\right] \quad (15)$$

The solution of Eq. (3) can be written as follows

$$T_i(z)=A_iz+B_i \quad (16)$$

By putting Eq. (16) into Eqs. (2)–(7)), the following expressions of A_i and B_i (i = 1 to 5) are derived

$$A_1=\frac{\frac{S_h}{k_1}\left[-\frac{t_2}{k_3}+\left(\frac{1}{k_3}-\frac{1}{k_4}\right)t_3+\left(\frac{1}{k_4}-\frac{1}{k_5}\right)t_4+\frac{t_5}{k_5}+\frac{1}{U_b}\right]}{\left[\left(\frac{1}{k_1}-\frac{1}{k_2}\right)t_1+\left(\frac{1}{k_2}-\frac{1}{k_3}\right)t_2+\left(\frac{1}{k_3}-\frac{1}{k_4}\right)t_3+\left(\frac{1}{k_4}-\frac{1}{k_5}\right)t_4+\frac{1}{k_5}t_5+\frac{1}{U_t}+\frac{1}{U_b}\right]} \quad (17)$$

$$A_2=\frac{\frac{S_h}{k_2}\left[-\frac{t_2}{k_3}+\left(\frac{1}{k_3}-\frac{1}{k_4}\right)t_3+\left(\frac{1}{k_4}-\frac{1}{k_5}\right)t_4+\frac{t_5}{k_5}+\frac{1}{U_b}\right]}{\left[\left(\frac{1}{k_1}-\frac{1}{k_2}\right)t_1+\left(\frac{1}{k_2}-\frac{1}{k_3}\right)t_2+\left(\frac{1}{k_3}-\frac{1}{k_4}\right)t_3+\left(\frac{1}{k_4}-\frac{1}{k_5}\right)t_4+\frac{1}{k_5}t_5+\frac{1}{U_t}+\frac{1}{U_b}\right]} \quad (18)$$

$$A_3=\frac{\frac{S_h}{k_3}\left[-\left(\frac{1}{k_1}-\frac{1}{k_2}\right)t_1-\frac{t_2}{k_2}-\frac{1}{U_t}\right]}{\left[\left(\frac{1}{k_1}-\frac{1}{k_2}\right)t_1+\left(\frac{1}{k_2}-\frac{1}{k_3}\right)t_2+\left(\frac{1}{k_3}-\frac{1}{k_4}\right)t_3+\left(\frac{1}{k_4}-\frac{1}{k_5}\right)t_4+\frac{1}{k_5}t_5+\frac{1}{U_t}+\frac{1}{U_b}\right]} \quad (19)$$

$$A_4=\frac{\frac{S_h}{k_4}\left[-\left(\frac{1}{k_1}-\frac{1}{k_2}\right)t_1-\frac{t_2}{k_2}-\frac{1}{U_t}\right]}{\left[\left(\frac{1}{k_1}-\frac{1}{k_2}\right)t_1+\left(\frac{1}{k_2}-\frac{1}{k_3}\right)t_2+\left(\frac{1}{k_3}-\frac{1}{k_4}\right)t_3+\left(\frac{1}{k_4}-\frac{1}{k_5}\right)t_4+\frac{1}{k_5}t_5+\frac{1}{U_t}+\frac{1}{U_b}\right]} \quad (20)$$

$$A_5=\frac{\frac{S_h}{k_5}\left[-\left(\frac{1}{k_1}-\frac{1}{k_2}\right)t_1-\frac{t_2}{k_2}-\frac{1}{U_t}\right]}{\left[\left(\frac{1}{k_1}-\frac{1}{k_2}\right)t_1+\left(\frac{1}{k_2}-\frac{1}{k_3}\right)t_2+\left(\frac{1}{k_3}-\frac{1}{k_4}\right)t_3+\left(\frac{1}{k_4}-\frac{1}{k_5}\right)t_4+\frac{1}{k_5}t_5+\frac{1}{U_t}+\frac{1}{U_b}\right]} \quad (21)$$

$$B_1=\frac{k_1A_1+U_tT_a}{U_t} \quad (22)$$

$$B_i=B_{i-1}+(A_{i-1}-A_i)t_{i-1} \quad for\ i=2\ to\ 5 \quad (23)$$

3. Validation

Kaplani and Kaplanis [2] have reported the experimentally measured cell temperature as 46.1 °C at tilt angle (β) = 30°, wind velocity (v_w) = 1 m/s, ambient temperature (T_a) = 20 °C and solar radiation on tilted surface (I_T) = 800 W/m^2 for silicon solar cell. For comparison, the cell temperature has been calculated using the proposed methodology which is 45.6 °C. Thus, the value computed using the proposed methodology differs from that of Kaplani and Kaplanis [2] by 0.5 °C. The mismatch is within the acceptable range as cell efficiency hardly varies for this small temperature difference.

4. Results and discussion

The temperature and efficiency of monocrystalline silicon, dye-sensitized and perovskite solar cells are calculated for various values of wind azimuth angle (wind direction), wind velocity, tilt angle of panel and solar radiation. The values of the parameters used for the calculations are presented in Table 1.

The optimum tilt angle is lower for places at lower latitudes and higher for higher latitudes. For building integration, tilt angle may kept as 90°. Thus, the variation of tilt angle (β) from 0° to 90° is shown in subsequent sections. However, while analysing the effect of other parameters, tilt angle is kept fixed as 45° which is near to optimum tilt angle for Cornwall, UK and is the mid value of the range of tilt angle ($0^\circ \leq \beta \leq 90^\circ$). Similarly, the variation in wind velocity (v_w) is shown in subsequent sections and while analysing the effect of other parameters, wind velocity is kept fixed as 4 m/s which is average wind velocity in sunny seasons at Cornwall, UK.

Table 1
Values of the parameters used for the calculations.

Parameters	Values		
	Monocrystalline Silicon Cell	Dye-sensitized Cell	Perovskite Cell
Material and thickness of 1st layer	Glass (3×10^{-3} m)	Glass (3×10^{-3} m)	Glass (3×10^{-3} m)
Material and thickness of 2nd layer	EVA (5×10^{-4} m)	Dye-sensitized TiO_2 (12×10^{-6} m)	TiO_2 (300×10^{-9} m)
Material and thickness of 3rd layer	Silicon (3×10^{-4} m)	Electrolyte (2×10^{-6} m)	Perovskite (250×10^{-9} m)
Material and thickness of 4th layer	EVA (5×10^{-4} m)	Platinum (300×10^{-9} m)	Spiro-OMeTAD (100×10^{-9} m)
Material and thickness of 5th layer	Tedlar (1×10^{-4} m)	Glass (3×10^{-3} m)	Silver (1×10^{-6} m)
T_a	30 °C	30 °C	30 °C
ε	0.85	0.85	0.85
η_{cell} (%)	25.3[1-0.0045(T_{cell}-25) + 0.085 ln (I_T/1000)] [4,19]	11.9[1-0.001(T_{cell}-40) + 0.085 ln (I_T/1000)]	22.1[1-0.005(T_{cell}-27) + 0.085 ln (I_T/1000)] 27 °C ≤ T_{cell} ≤ 50 °C [17,19]
$(\tau\alpha)_{eff}$	0.9	0.7	0.7

4.1. Effect of wind azimuth angle

The variations in temperature and efficiency of cells with wind azimuth angle (γ_w) are plotted in Figs. 2 and 3 respectively keeping $\beta = 45°$, $I_T = 1000\ W/m^2$ and $v_w = 4$ m/s. The results show that as the wind azimuth angle increases from 0° to 90°, the temperature of the cell increases from 51.8 °C to 58.2 °C for monocrystalline silicon solar cell, from 48.4 °C to 53.9 °C for dye-sensitized solar cell and from 45.5 °C to 50.7 °C for perovskite solar cell and the corresponding efficiency of the cell decreases from 22.3% to 21.5% for monocrystalline silicon, from 11.8% to 11.7% for dye-sensitized solar cell and from 20.1% to 19.5% for perovskite solar cell. This is due to the fact that when wind azimuth angle is 0°, the wind direction is normal to surface which leads to higher heat losses due to forced convection and thus lesser temperature and higher efficiency. The results also show that the temperature of monocrystalline silicon solar cell is higher than that of perovskite and dye-sensitized solar cells due to higher heat generation.

4.2. Effect of wind velocity

The variations in temperature and efficiency of cells with wind velocity (v_w) are plotted in Figs. 4 and 5 respectively keeping $\beta = 45°$, $I_T = 1000\ W/m^2$ and $\gamma_w = 0°$. The results show that as the wind velocity increases from 0.5 m/s to 6 m/s, the temperature of the cell decreases from 61.4 °C to 49.3 °C for monocrystalline silicon solar cell, from 56.6 °C to 46.3 °C for dye-sensitized solar cell and from 53.3 °C to 43.7 °C for perovskite solar cell and the corresponding efficiency of the cell increases from 21.2% to 22.5% for monocrystalline silicon, from 11.7% to 11.8% for dye-sensitized and from 19.2% to 20.3% for perovskite solar cell. This is due to the fact that the increase in wind velocity leads to increment in heat losses which results in decrement in the temperature of the cell and, thus, increment in efficiency.

4.3. Effect of tilt angle of panel

The variations in temperature and efficiency of cells with tilt of panel (β) are plotted in Figs. 6 and 7 respectively keeping $\gamma_w = 0°$, $I_T = 1000\ W/m^2$ and $v_w = 4$ m/s. If the change in incident solar radiation will be considered along with the change in tilt, it will result as combined effect of both. In that case, it will be hard to find the effect of individual that whether something is happened due to change in tilt angle or change in incident solar radiation. Thus, the effects of both are analysed separately in Sections 4.3 and 4.4 respectively. The results show that as tilt of panel increases from 0° to 90°, the temperature of the cell decreases from 57.8 °C to 50.5 °C for monocrystalline silicon solar cell, from 53.5 °C to 47.3 °C for dye-sensitized solar cell and from 50.3 °C to 44.6 °C for perovskite solar cell and the corresponding efficiency of the cell increases from 21.6% to 22.4% for monocrystalline silicon, from 11.7% to 11.8% for dye-sensitized solar cell and from 19.5% to

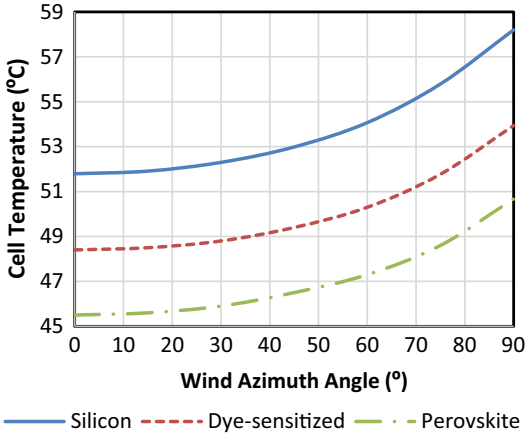

Fig. 2. Variation in the temperature of the cells with wind azimuth angle (γ_w) i.e. wind direction.

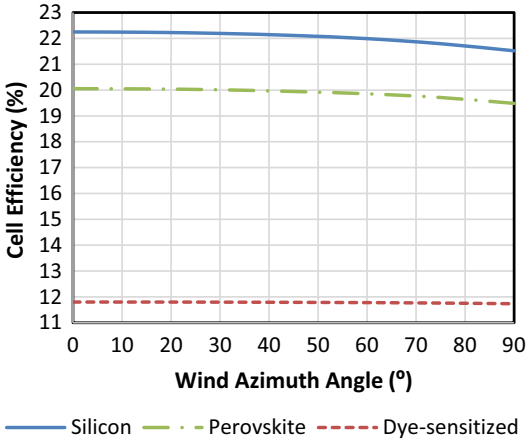

Fig. 3. Variation in the efficiency of the cells with wind azimuth angle (γ_w) i.e. wind direction.

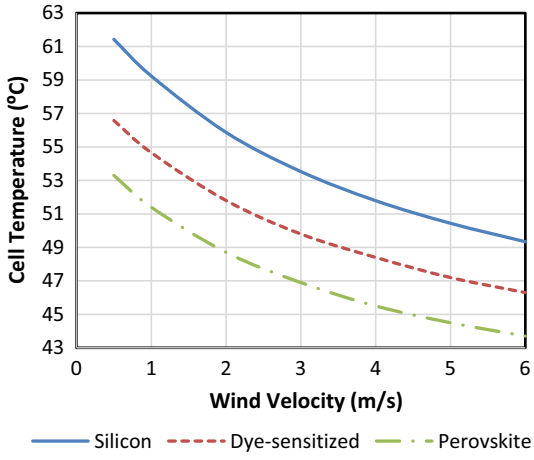

Fig. 4. Variation in the temperature of the cells with wind velocity (v_w).

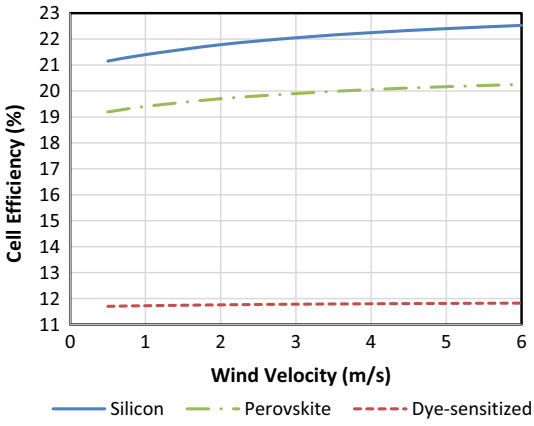

Fig. 5. Variation in the efficiency of the cells with wind velocity (v_w).

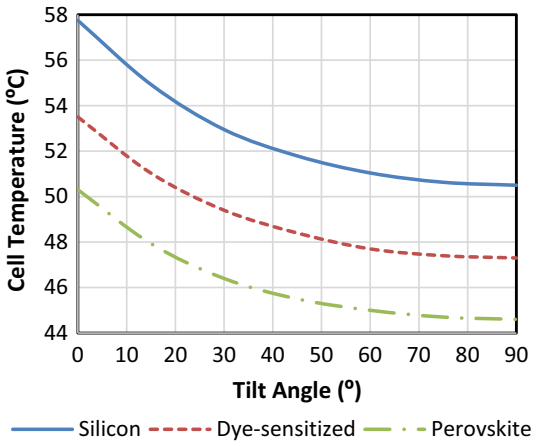

Fig. 6. Variation in the temperature of cells with the tilt angle of panel (β).

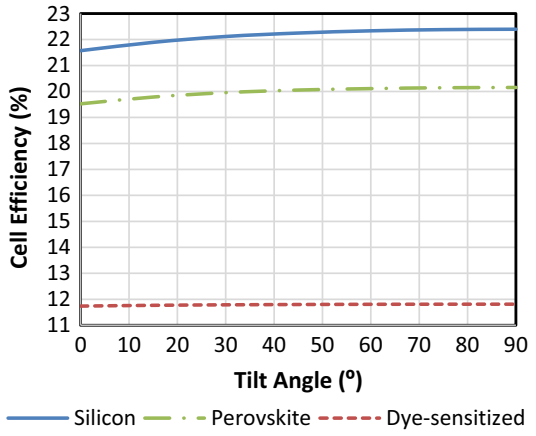

Fig. 7. Variation in the efficiency of cells with the tilt angle of panel (β).

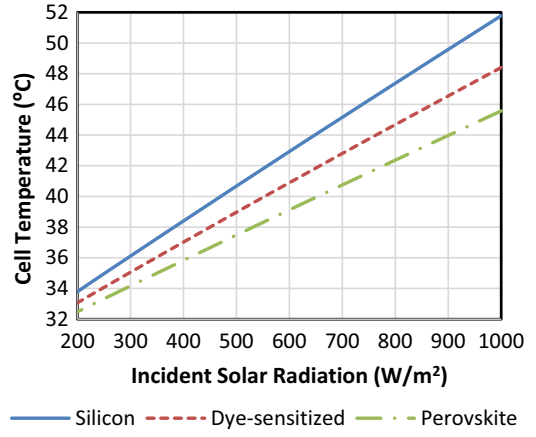

Fig. 8. Variation in the temperature of cells with incident solar radiation (I_T).

20.2% for perovskite solar cell. This is due to the fact that the higher tilt angle leads to larger heat losses due to forced convection which results in lesser temperature of the cell and, thus, higher efficiency.

4.4. Effect of incident solar radiation

The variations in temperature and efficiency of cells with incident solar radiation (I_T) are plotted in Figs. 8 and 9 respectively

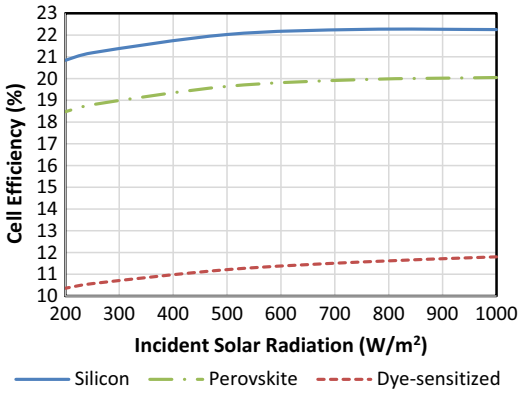

Fig. 9. Variation in the efficiency of cells with incident solar radiation (I_T).

keeping $\beta = 45°$, $\gamma_w = 0°$ and $v_w = 4$ m/s. The results show that as the incident solar radiation increases from 200 to 1000 W/m^2, the temperature of the cell increases from 33.8 °C to 51.8 °C for monocrystalline silicon solar cell, from 33.1 °C to 48.4 °C for dye-sensitized solar cell and from 32.5 °C to 45.5 °C for perovskite solar cell and the corresponding efficiency of the cell increases from 20.8% to 22.3% for monocrystalline silicon, from 10.4% to 11.8% for dye-sensitized solar cell and from 18.5% to 20.1% for perovskite solar cell. This is due to the fact that the increase in solar radiation leads to increase in heat generation and, thus, increase in temperature of the cell. Increase in insolation has its own positive effect on efficiency which dominates over the negative effect of rise in temperature. Thus, efficiency increases with insolation. Since heat generation in monocrystalline silicon solar cell is higher than the other studied cells, the temperature of silicon cell remains higher in any operating condition. Thus, ranking of cells remains same in all the sections from 4.1 to 4.4.

5. Conclusions

In the current work, the performance of perovskite and dye-sensitized solar cells in operating conditions has been analysed and compared with monocrystalline silicon solar cell. An analytical expression has been derived that gives correlation between cell's performance and operating conditions. For validation purpose, the values of temperature for silicon solar cell are computed using the proposed methodology and it is found that they differ from those of Kaplani and Kaplanis [2] by less than 0.5 °C. The effects of wind direction (wind azimuth angle), wind velocity, tilt angle of panel and solar radiation on the temperature and efficiency of monocrystalline silicon, perovskite and dye-sensitized solar cells have been analysed. The conclusions are as follows

(i) Higher heat generation in monocrystalline silicon solar cell leads to higher temperature as compared to perovskite and dye-sensitized solar cell.
(ii) For monocrystalline silicon cell, the increase in wind azimuth angle from 0° to 90° leads to increase in temperature of the cell from 51.8 °C to 58.2 °C and decrease in the efficiency from 22.3% to 21.5%.
The increase in wind velocity from 0.5 m/s to 6 m/s leads to decrease in temperature of the cell from 61.4 °C to 49.3 °C and increase in the efficiency from 21.2% to 22.5%.
The increase in the tilt of panel from 0° to 90° leads to decrease in temperature of the cell from 57.7 °C to 50.5 °C and increase in the efficiency of cell from 21.6% to 22.4%.
The increase in solar radiation from 200 to 1000 W/m^2 leads to increase in temperature of the cell from 33.8 °C to 51.8 °C and increase in the efficiency of cell from 20.8% to 22.3%.

(iii) For perovskite solar cell, the increase in wind azimuth angle from 0° to 90° leads to increase in temperature of the cell from 45.5 °C to 50.7 °C and decrease in the efficiency from 20.1% to 19.5%.
The increase in wind velocity from 0.5 m/s to 6 m/s leads to decrease in temperature of the cell from 53.3 °C to 43.7 °C and increase in the efficiency of cell from 19.2% to 20.3%.
The increase in the tilt of panel from 0° to 90° leads to decrease in temperature of the cell from 50.3 °C to 44.6 °C and increase in the efficiency of cell from 19.5% to 20.2%.
The increase in solar radiation from 200 to 1000 W/m^2 leads to increase in temperature of the cell from 32.5 °C to 45.5 °C and increase in the efficiency of cell from 18.5% to 20.1%.

(iv) For dye-sensitized solar cell, the increase in wind azimuth angle from 0° to 90° leads to increase in temperature of the cell from 48.4 °C to 53.9 °C and decrease in the efficiency from 11.8% to 11.7%.
The increase in wind velocity from 0.5 m/s to 6 m/s leads to decrease in temperature of the cell from 56.6 °C to 46.3 °C and increase in the efficiency of cell from 11.7% to 11.8%.
The increase in the tilt of panel from 0° to 90° leads to decrease in temperature of the cell from 53.5 °C to 47.3 °C and increase in the efficiency of cell from 11.7% to 11.8%.
The increase in solar radiation from 200 to 1000 W/m^2 leads to increase in temperature of the cell from 33.1 °C to 48.4 °C and increase in the efficiency of cell from 10.4% to 11.8%.

Thus, from the current work, the service providers can evaluate the performance of the system beforehand for the specific weather conditions of their respective locations which will help them calculate the area required to meet the demand. The analytical expression derived in the manuscript considers all the layers of the cells and this is its uniqueness. It will help researchers and manufacturers plug in the properties of different layers of their own cells to analyse them.

Acknowledgment

The authors gratefully acknowledge the financial support from EPSRC-DST funded Reliable and Efficient System for Community Energy Solution - RESCUES project (EP/K03619X/1). In support of open access research, all underlying article materials (such as data, samples or models) can be accessed upon request via email to the corresponding author.

References

[1] E. Skoplaki, J.A. Palyvos, Operating temperature of photovoltaic modules: A survey of pertinent correlations, Renew. Energy 34 (2009) 23–29.
[2] E. Kaplani, S. Kaplanis, Thermal modelling and experimental assessment of the dependence of PV module temperature on wind velocity and direction, module orientation and inclination, Sol. Energy 107 (2014) 443–460.
[3] E. Skoplaki, A.G. Boudouvis, J.A. Palyvos, A simple correlation for the operating temperature of photovoltaic modules of arbitrary mounting, Sol. Energy Mater. Sol. Cells 92 (2008) 1393–1402.
[4] E. Skoplaki, J.A. Palyvos, On the temperature dependence of photovoltaic module electrical performance: A review of efficiency/power correlations, Sol. Energy 83 (2009) 614–624.
[5] Z.H. Lu, Q. Yao, Energy analysis of silicon solar cell modules based on an optical model for arbitrary layers, Sol. Energy 81 (2007) 636–647.
[6] A.D. Jones, C.P. Underwood, A thermal model for photovoltaic systems, Sol. Energy 70 (2001) 349–359.
[7] S. Armstrong, W.G. Hurley, A thermal model for photovoltaic panels under varying atmospheric conditions, Appl. Therm. Eng. 30 (2010) 1488–1495.
[8] M. Grätzel, Dye-sensitized solar cells, J. Photochem. Photobiol., C 4 (2003) 145–153.
[9] S.R. Raga, F. Fabregat-Santiago, Temperature effects in dye-sensitized solar cells, Phys. Chem. Chem. Phys. 15 (2013) 2328–2336.
[10] P.J. Sebastian, A. Olea, J. Campos, J.A. Toledo, S.A. Gamboa, Temperature dependence and the oscillatory behavior of the opto-electronic properties of a dye-sensitized nanocrystalline TiO_2 solar cell, Sol. Energy Mater. Sol. Cells 81 (2004) 349–361.
[11] H. Pettersson, T. Gruszecki, L. Johansson, P. Johander, Manufacturing method for monolithic dye-sensitised solar cells permitting long-term stable low-power modules, Sol. Energy Mater. Sol. Cells 77 (2003) 405–413.
[12] S. Chen, Y. Huang, J. Weng, X. Fan, L. Mo, B. Pan, S. Dai, Numerical model analysis of thermal performance for a dye-sensitized solar cell module, J. Phys. D Appl. Phys. 46 (2013) 485106.
[13] B. Pan, S. Chen, Y. Huang, Z. Shao, J. Weng, S. Xiao, S. Dai, Design and thermal analysis of a water-cooled DSC module, Sci. China Technol. Sci. 59 (2016) 1276–1282.
[14] M. Berginc, U.O. Krasovec, M. Jankovec, M. Topic, The effect of temperature on the performance of dye-sensitized solar cells based on a propyl-methyl-imidazolium iodide electrolyte, Sol. Energy Mater. Sol. Cells 91 (2007) 821–828.
[15] M. Berginc, U.O. Krasovec, M. Hocevar, M. Topic, Performance of dye-sensitized solar cells based on Ionic liquids: Effect of temperature and iodine concentration, Thin Solid Films 516 (2008) 7155–7159.
[16] B. Tripathi, P. Yadav, M. Kumar, Effect of varying illumination and temperature on steady-state and dynamic parameters of dye-sensitized solar cell using AC impedance modelling, Int. J. Photoenergy (2013) 646407.
[17] H. Zhang, X. Qiao, Y. Shen, M. Wang, Effect of temperature on the efficiency of organometallic perovskite solar cells, J. Energy Chem. 24 (2015) 729–735.
[18] L. Cojocaru, S. Uchida, Y. Sanehira, V. Gonzalez-Pedro, J. Bisquert, J. Nakazaki, T. Kubo, H. Segawa, Temperature effects on the photovoltaic performance of planar structure perovskite solar cells, Chem. Lett. 44 (2015) 1557–1559.
[19] NREL efficiency chart <http://www.nrel.gov/pv/assets/images/efficiency_chart.jpg> (accessed 27.12.2016).